Catal Lett (2009) 129:303–311
DOI 10.1007/s10562-009-9853-x

Cyclohexane Oxidation Over Size-Uniform Au Nanoparticles (SBA-15 hosted) in a Continuously Stirred Tank Reactor Under Mild Conditions

Li Li · Chen Jin · Xiaochen Wang · Weijie Ji · Yi Pan · Theo van der Knaap · Roland van der Stoel · C. T. Au

Received: 29 December 2008 / Accepted: 1 January 2009 / Published online: 21 January 2009

Abstract Cyclohexane oxidation was operated in a continuously stirred tank reactor at system pressures of 0.6–1.0 MPa under an air-like O_2/N_2 atmosphere (rather than pure O_2). Catalytic performance was investigated over Au nanoparticles (size: 3–8 nm) hosted by SBA-15 as well as Au particles (>60 nm) deposited on MCM-41, and high turnover frequencies of desired products were detected over the former. Based on intrinsic activities of representative catalysts, we derived a size-sensitivity feature of cyclohexane oxidation over Au particles.

Keywords Mesoporous material · Gold · Nanostructure · Oxidation · Cyclohexane

1 Introduction

The oxidation of cyclohexane (CHX) is carried out in caprolactam manufacture for large-scale production of cyclohexanol (CHOL) and cyclohexanone (CHONE). In the absence of a catalyst, CHX autoxidation is known to proceed via a radical chain mechanism with cyclohexyl–hydroperoxide (CHHP) being the key product [1]. In the past decades, scientists have been working on the catalysis of CHX oxidation [2]; catalysts such as VPO [3], chemically modified inorganic matrixes [4], Ti-containing molecular sieves [5–8], Fe, Mn, Co-$AlPO_4$ and Fe-ZSM-5 [9], (Cr)MCM-41 [10] and metalloporphyrins [11–13] have been investigated. Since the pioneer work of Haruta [14, 15], gold nanoparticles (NPs) have been studied as catalysts for a number of reactions [16–21]. In particular, Au particles dispersed on ZSM-5 [22], mesoporous materials [23–25], and Al_2O_3 [26] were explored for liquid-phase CHX oxidation. In the study reported herein, we used Au NPs hosted by SBA-15 as catalysts for CHX oxidation. We selected SBA-15 as the host material because it has well-ordered large hexagonal porosities with high thermal stability and surface area [27]. The following aspects have been emphasized: (1) The reactions were operated under mild conditions in an O_2/N_2 mixture (one similar to air, rather than pure O_2, system pressure = 0.6–1.0 MPa); (2) a continuously stirred tank reactor (CSTR) of large capacity (1 L) was adopted for the first time to increase CHX inventory and to maintain system pressure (within 0.001 MPa variation); (3) two preparation methods for the synthesis of SBA-15 hosted Au NPs, viz. one-pot and 3-aminopropyl-trimethoxysilane (APTS)-modified synthesis, were compared for their influence on the characteristics and catalytic performances of the derived Au NPs; (4) high turnover frequencies (TOFs) were obtained and a size-sensitivity feature of CHX oxidation demonstrated.

L. Li · C. Jin · X. Wang · W. Ji (✉) · Y. Pan (✉)
Key Laboratory of Mesoscopic Chemistry, MOE,
School of Chemistry and Chemical Engineering,
Department of Chemistry, Nanjing University,
210093 Nanjing, China
e-mail: jiwj@nju.edu.cn

Y. Pan
e-mail: yipan@nju.edu.cn

T. van der Knaap · R. van der Stoel
DSM Fibre Intermediates, Poststraat 1, P.O. Box 43,
6130 AA Sittard, The Netherlands

C. T. Au
Department of Chemistry, Hong Kong Baptist University,
Kowloon Tong, Hong Kong, China

2 Experimental

2.1 Catalyst Preparation

There were three types of Au-containing catalysts, namely, Au/SBA-15, Au/APTS-SBA-15, and Au/MCM-41. One-pot synthesis of 1%Au/SBA-15 catalyst was performed according to the following procedures: (1) 0.42 mmol g of P_{123} [$EO_{20}PO_{70}EO_{20}$, poly(ethylene glycol)-block-poly(propylene glycol)-block-poly(ethylene glycol), average molecular weight 5,800, Aldrich; the template used for preparing mesoporous silica] was dissolved in 1.01 mol distilled water under stirring at room temperature (RT); (2) 2 M HCl solution (70.6 mL) was added and the mixture was stirred at 40 °C for 4 h; (3) $HAuCl_4$ solution of 3.1 mL (2.43×10^{-2} mol/L) was added; (4) after 1 h, 2.47×10^{-2} mol tetraethylorthosilicate (TEOS) was added under vigorous stirring; (5) after ageing at 40 °C for 24 h, the mixture was transferred into a Teflon lined autoclave and kept at 95 °C for 48 h; (6) the solid product was collected by filtration, washed with repeated cycles of distilled water and ethanol, and dried in air at RT; and (7) the solid precursor was calcined in air at 550 °C for 4.5 h and then reduced in a flow of 5% H_2/Ar (40 mL/min) at 200 °C for 4 h. By changing the amount of $HAuCl_4$ solution, the 0.5%Au/SBA-15 and 1.5%Au/SBA-15 samples were prepared in a similar manner.

The 1%Au/APTS-SBA-15 catalyst was prepared as follows: (1) Synthesis of SBA-15 [TEOS:P123:HCl:H_2O = 1:0.017:5.71:192 (*n*/*n*)]:P123 was dissolved in water and HCl solution was added, and the mixture was stirred at 40 °C for 4 h. Then TEOS was added and the mixture was aged for 24 h. The as-obtained mixture was hydrothermally treated at 95 °C for 48 h in an autoclave. The solid product was collected, washed repeatedly in cycles of distilled water and ethanol, and dried in air at RT, followed by calcination in air at 550 °C for 6 h. (2) Modification of as-prepared SBA-15 with APTS: 1 g SBA-15 was added to an APTS solution (1.70×10^{-3} mol APTS + 0.28 mol toluene), and the mixture was heated at 80 °C with a water-condenser for 6 h. The solid was collected, washed with ethanol, and dried in air at RT to obtain the APTS-modified SBA-15. (3) Preparation of Au/APTS-SBA-15: APTS-SBA-15 was added to a $HAuCl_4$ solution of 1 mmol/L at RT and the mixture was heated at 80 °C with a water-condenser for 5 h. The solid product was filtered out, fully washed with distilled water (until Cl^- free) and then washed with ethanol. The calcination and reduction procedures were similar to those adopted for preparation of 1%Au/SBA-15.

The 1%Au/MCM-41 was prepared by the following steps: (1) MCM-41 precursor was synthesized according to the procedures reported previously [28, 29]; and (2) the derived precursor was added to a $HAuCl_4$ solution of 1 mmol/L and the mixture was heated at 80 °C with a water-condenser for 24 h; (3) the solid product was filtered out, washed repeatedly in cycles of water and ethanol, and dried at RT; (4) the collected material (2 g) was further refluxed in a HCl/EtOH solution at 78 °C for 24 h (to remove the template); and (5) the sample was directly reduced in a flow of 5% H_2/Ar (40 mL/min) at 200 °C for 4 h (without prior calcination as in the previous cases).

2.2 Catalyst Evaluation

The CSTR system adopted in the present study consists of (1) reactor with a Ti alloy vessel which was proved to be inactive for CHX oxidation; (2) two series of condensers; (3) small scale PC-DCS system comprising the computer, the signal-circuit regulator and the programmable controllers for the computer-control of pressure, temperature, and stirring speed; and (4) apparatus for GC analysis.

The reaction temperature and system pressure was essentially in the range of 140–150 °C and 0.6–1.0 MPa. The stirring speed was 500 or 650 rpm. For an inventory of 1.85 mol CHX, 0.5 g catalyst was used. The flow rate of O_2 and N_2 was 80 and 320 mL/min, respectively. During initial heating, only N_2 was fed into the reactor (to minimize CHX autoxidation). At a designated temperature, O_2 was introduced and the reaction started. After a reaction of designated period, the reactor was opened and liquid sample was collected (there was no collection of sample during the reaction) by centrifugation and analyzed by FID of Agilent 6890N GC with CP SIL 8 CB (30 m × 0.32 mm × 1.2 μm) capillary column. A PTV (programmed temperature vaporization) injector was used to measure unstable intermediates/products such as CHHP. The temperature program of oven was 40 °C (1 min) (at 5°C/min) to 280 °C (1 min), while that of PTV injector 70 °C (0.05 min) (at 10 °C/s) to 255 °C (5 min). The off-gases were analyzed on-line by TCD with packed column of Hayesep D (100/120 mesh, 6.1 m) and oven temperature program of 30 °C (5 min) (at 5 °C/min) to 150 °C.

2.3 Catalyst Characterization

Specific surface area, pore volume, and pore size distribution of samples were obtained based on N_2 adsorption–desorption isotherms measured at −196 °C over an ASAP-2020 instrument. X-ray diffraction was performed on an X'Pert Pro diffractometer with Cu Kα radiation in the 2θ range of 3–80°. The TEM images were taken on a JEOL-JEM-1010 transmission electron microscope. XPS measurement was performed on a VG ESCALAB MK II spectrometer using Mg Kα radiation.

3 Results and Discussion

3.1 Catalytic Performance

Figure 1 shows the CHX conversions over the catalysts under selected conditions. Over 1%Au/SBA-15 at 0.6 MPa and 150 °C (Entry C, 500 rpm), CHX conversion was 14.4% after a reaction period of 3 h, whereas at 1.0 MPa and 140 °C (Entry D, 500 rpm), CHX conversion was ~16% after 4 h. One can see that with rise of pressure, there was an increase in CHX conversion (Entries B and C). Also, at 1.0 MPa and 150 °C with reaction period extended from 3 to 6 h, there was a rise of CHX conversion from ~15 to ~20% (Entries A and B). Figure 1 also indicated that with a change of stirring speed from 500 to 650 rpm, there was a decrease in CHX conversion (Entries D and E). Similar observation was also made for an autoxidation system (without catalyst) operated in the same CSTR. For the configuration of the CSTR applied, the gas outlets are close to the head of stirrer. At higher stirring speed, there might be small gap between the liquid/catalyst-containing liquid and the gas outlets, resulting in poorer contact at the gas–liquid or the gas–liquid–solid interfaces. Over 1%Au/APTS-SBA-15 at 1.0 MPa and 150 °C, CHX conversion was 15.5% after 3 h. Over 1%Au/MCM-41 under comparable conditions (3 h, 1.5 MPa, and 145 °C), CHX conversion was less than 1%. Over Au/SBA-15 and Au/APTS-SBA-15, a change of Au loading from 0.5 to 1.5% or a variation of reaction temperature between 140 °C (4 h) and 150 °C (3 h) showed slight effect on CHX conversion (Fig. 2).

High CHX conversions (28–32%, with a period of 6 h-reaction) have been reported by Zhu et al. [25] over Au/IL-SBA-15 (ion liquid-modified), and Au/SH-SBA-15 (thiol-modified) catalysts. Note that the catalysts of Zhu et al. were not subject to calcination and reduction prior to reaction, and the impact of functional groups on CHX oxidation is uncertain. In order to estimate the extent of autoxidation in Au-catalyzed reactions, we conducted CHX oxidation reactions in the absence of a catalyst (Fig. 3). One can see that autoxidation is negligible at 145 °C but becomes significant at 170 °C (a temperature adopted in industry). We also observed that CHX oxidation over SBA-15 and MCM-41 was negligible in the 140–150 °C range. Accordingly, we operated the Au-catalyzed reactions at a temperature no higher than 150 °C. The CHX conversions as well as the selectivities to the desired products (CHOL + CHONE + CHHP) with time on stream were presented in Fig. 4. One can observe that the conversion and selectivity are dependent each other. With increasing

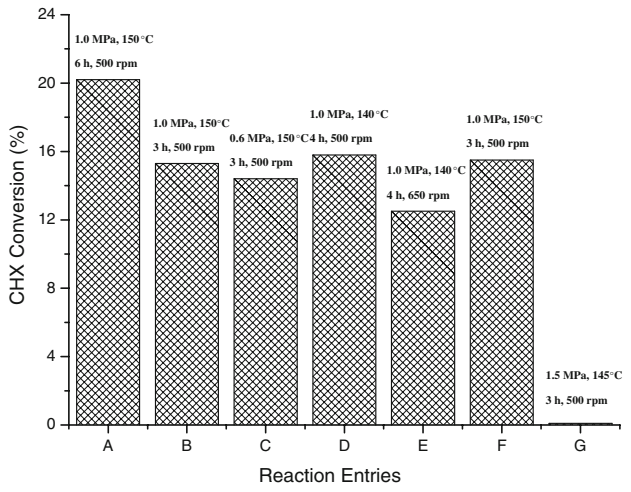

Fig. 1 CHX conversions over 1%Au/SBA-15 (*Entries A–E*), 1%Au/APTS-SBA-15 (*Entry F*), and 1%Au/MCM-41 (*Entry G*)

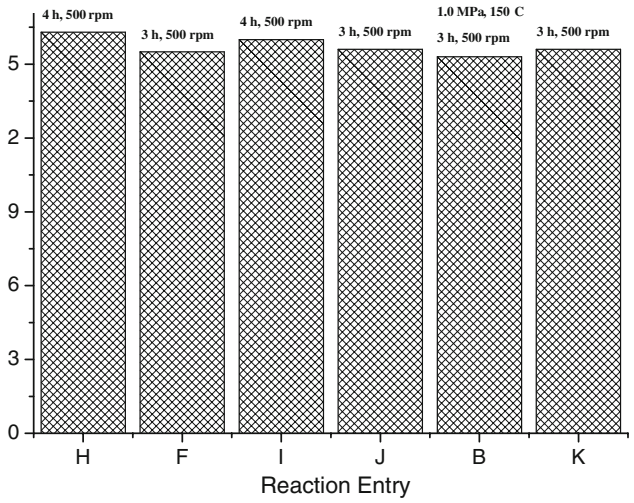

Fig. 2 CHX conversions over 0.5%Au/APTS-SBA-15 (*Entry H*), 1.0%Au/APTS- SBA-15 (*Entry F*), 0.5%Au/SBA-15 (*Entries I* and *J*), 1.0%Au/SBA-15 (*Entry B*), and 1.5%Au/SBA-15 (*Entry K*)

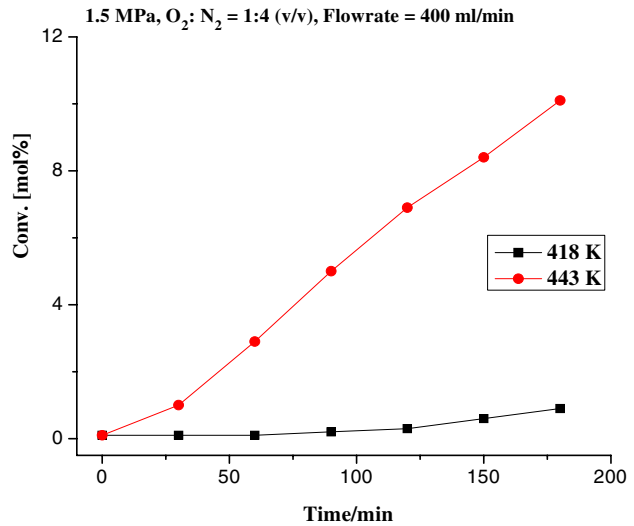

Fig. 3 CHX conversions obtained via auto-oxidation

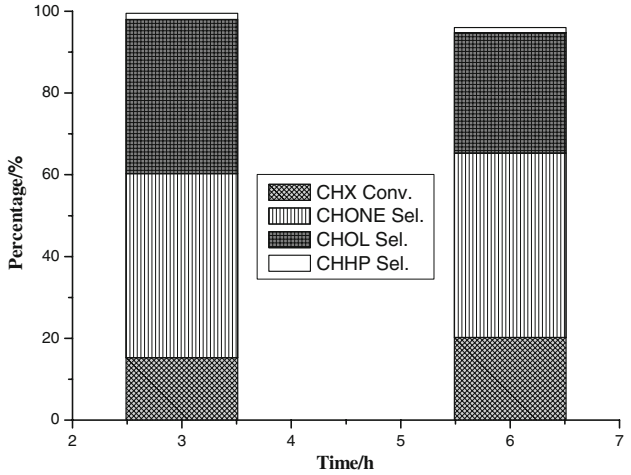

Fig. 4 CHX conversions and selectivities to the desired products (CHOL + CHONE + CHHP) with time. Reaction temperature: 150 °C; pressure: 1.0 MPa; stirring speed: 500 rpm

conversion beyond 20%, selectivity decreases steadily below 76%. Nowadays the criterion of reaction selectivity becomes more important, and the low selectivity of CHX oxidation (<76%) is certainly undesirable. Therefore, in the present study the CHX conversion is essentially controlled in the range of 10–20%, with an effort to enhance the selectivity.

As illustrated in Table 1, product distribution over 1%Au/SBA-15 can be obviously affected by reaction variables. In general, with lowering of reaction temperature from 150 to 140 °C, there is enhanced selectivity (85.3 mol%) to desired products (i.e. CHOL + CHONE + CHHP), and in particular an enlarged CHONE/CHOL (denoted as K/A hereinafter) ratio (1.5). In the cases of CHX autoxidation and metalloporphyrin-catalyzed reactions, K/A ratio is always smaller than 1.0. We consider that the preferential formation of CHONE against CHOL is an attractive feature for CHX oxidation over Au NPs. From Table 1, one can see that with reaction extended from 3 to 6 h, there is an overall decline of selectivity to (CHOL + CHONE + CHHP) (from 84.5 to 75.8 mol%); the variation in CHONE, CHHP, and C_5/C_6 acids selectivity is slight but decrease in CHOL selectivity is obvious. The results suggest that with time on stream it is CHOL rather than CHONE and C5/C6 acids that is converted to by-products.

It is worth pointing out that with decline in system pressure from 1.0 to 0.6 MPa, selectivity to CHOL and C_6 acids increases while that to CHONE decreases (consequently a decline of K/A ratio from 1.2 to 0.8). The results suggest that with decreasing system pressure, there was a notable shift in reaction pathway. Stirring speed also has an effect on product distribution. A rise of stirring speed from 500 to 650 rpm causes a considerable decline in CHONE selectivity (selectivity to C5 and C6 acids is also somewhat reduced) but increase in CHOL and CHHP selectivity. It is also obvious that with higher stirring speed there is a decrease in degree of oxidation, in agreement with the interpretation of conversion data shown in Fig. 1. Note that similar product distributions (Table 1, Entry B vs. Entry F, with CHHP being only slightly lower) were observed over 1%Au/SBA-15 and 1%Au/APTS-SBA-15. On the other hand, distribution of liquid-phase products over 1%Au/MCM-41 is drastically different (Table 1, Entry G): only small amount of CHONE (12.8%) was obtained and there was no formation of CHOL and CHHP. We observed that over Au/SBA-15 catalysts with variation of Au from 0.5 to 1.0% and then to 1.5%, K/A ratio (150 °C, 3 h) first increased (from 0.8 to 1.2) and then decreased (to 0.9), meanwhile overall (CHONE + CHOL + CHHP) selectivity changed from 75.6 to 84.2% and then to 79.8%. We hence considered that the optimal loading of Au for the target reaction is 1.0%.

The O_2 and CO concentrations in off-gas were measured for better understanding of the reaction. It was observed

Table 1 Distribution of liquid-phase products and K/A ratios

Selectivity	Entry[a] (mol%)									
	A	B	C	D	E	F	G	I	J	K
CHONE	45.1	45.0	33.2	50.2	41.6	46.8	12.8	42.5	31.6	36.3
CHOL	29.4	37.7	41.3	33.4	41.1	36.8	0	37.7	41.6	41.9
CHHP	1.3	1.5	1.9	1.3	4.5	0.2	0	1.4	2.4	1.6
C5 acids	3.8	3.8	3.9	2.4	1.4	3.6	0	3.2	3.7	3.3
C6 acids	3.3	2.7	8.2	2.5	1.5	2.0	11.0	4.4	7.7	5.7
Others	17.1	10.0	11.5	9.8	9.9	10.6	76.2	10.8	13.0	11.2
K/A	1.5	1.2	0.8	1.5	1.0	1.3	–	1.1	0.8	0.9

[a] For Entries A–E, 1%Au/SBA-15 was used; for Entries F and G, 1%Au/APTS-SBA-15 and 1%Au/MCM-41 was used, respectively; for Entries I and J, 0.5%Au/SBA-15 was used, and for Entry K, 1.5%Au/SBA-15 was adopted. O_2/N_2 = 1:4 (v/v), total flow rate = 400 mL min^{-1}. Reaction conditions are the same as those indicated in Figs. 2 and 3

that at reaction temperatures of 150 and 140 °C over 1.0%Au/SBA-15, O_2 concentration was 7.4 and 16.6% after 2 h, and CO concentration was 4.2 and 1.5% after 3 h, respectively. In other words, CHX oxidation occurred more readily at 150 °C. On the other hand, at higher stirring speed of 650 rpm, relatively higher O_2 concentration (18.9% at 140 °C after 2 h) and lower CO concentration (0% at 140 °C after 2 h) were detected, in accord with the lower degree of oxidation at higher stirring speed shown in Fig. 1. Furthermore, the reaction over 1%Au/APTS-SBA-15 showed higher CO concentration in off-gas than that over 1%Au/SBA-15, especially at the early stage of reaction (1.4 vs. 0% after 1 h), suggesting that 1%Au/APTS-SBA-15 is more reactive than 1%Au/SBA-15 for deep oxidation.

3.2 Catalyst Characterization

3.2.1 N_2 Adsorption–desorption

In order to understand the reaction behaviors, the 0.5 and 1.0%Au/SBA-15 and 0.5 and 1.0%Au/APTS-SBA-15 catalysts were subject to N_2 adsorption–desorption measurements, and the results are shown in Fig. 5 and also summarized in Table 2. All the samples show typical D-type adsorption–desorption isotherms, indicating the presence of mesopore structures. The 0.5%Au/APTS-SBA-15 and 1.0%Au/APTS-SBA-15 catalysts are comparatively lower in surface area and pore volume but slightly bigger in pore diameter, suggesting that (1) with APTS-surface modification of SBA-15, it is likely to have more Au NPs positioned inside the channels, resulting in enhanced blocking of channels (especially the narrow ones); and (2) the Au NPs in APTS-modified SBA-15 are probably relatively bigger than those in Au/SBA-15 (without APTS-modification). Zhu et al. [25] reported more significant drop in BET surface area and pore volume over the Au/APS-SBA-15 and Au/HS-SBA-15 samples, likely to be a result of higher Au loadings.

3.2.2 TEM

The TEM images of representative samples confirm the above deductions (Fig. 6). First of all, it is clear that the hexagonally mesoporous structure of SBA-15 is maintained. The particle diameters of 1%Au/SBA-15 (Fig. 6b)

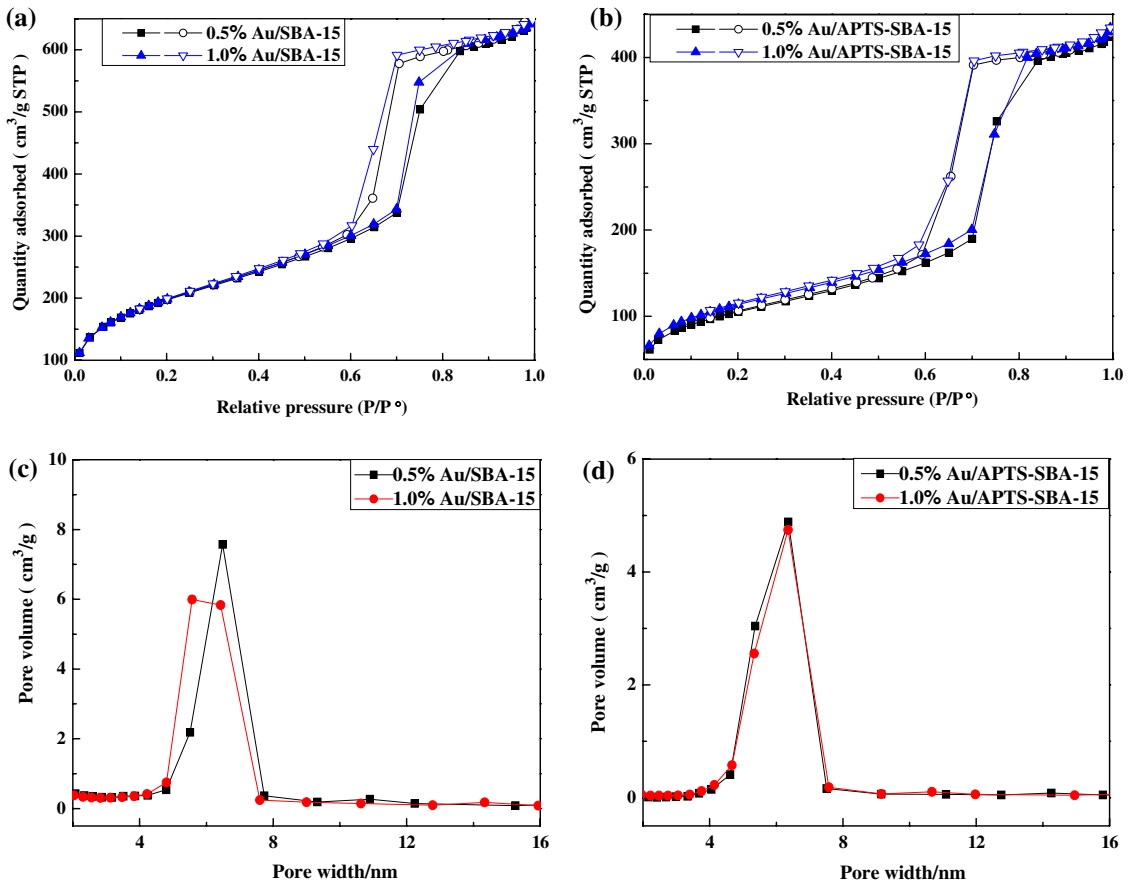

Fig. 5 N_2 adsorption–desorption isotherms of **a** 0.5% & 1%Au/SBA-15, and **b** 0.5% & 1%Au/APTS-SBA-15; pore size distribution of **c** 0.5% & 1%Au/SBA-15, and **d** 0.5% & 1%Au/APTS-SBA-15

Table 2 Surface area, average pore width, and pore volume of the supported Au catalysts

Sample	Surface area (m^2/g)	Average pore width (nm)	Pore volume (cm^3/g)
0.5%Au/SBA-15	712	5.8	1.05
1.0%Au/SBA-15	716	5.5	1.04
0.5%Au/APTS-SBA-15	378	6.2	0.68
1.0%Au/APTS-SBA-15	410	6.1	0.69

and 1%Au/APTS-SBA-15 (Fig. 6d) are essentially in the range of 3–8 nm. In the case of 1%Au/SBA-15, there is higher percentage of Au particles in the range of 5–6 nm (55%) while lower percentages in the range of 4–5 nm (20%) and 6–7 nm (10%). In the case of 1%Au/APTS-SBA-15, there is comparatively lower proportion of Au particles in the range of 5–6 nm (36%) and higher fractions in the range of 4–5 nm (30%) and 6–7 nm (30%). In the latter case, most of the Au NPs (mean particle size = 5.6 nm) are highly dispersed in a uniform manner inside the channels of SBA-15, plausibly a result of surface modification of SBA-15 with APTS. Zhu et al. [25] found that the surface property of SBA-15 can have a strong effect on the size of Au particles. Among the Au/APS-SBA-15, Au/HS-SBA-15, and Au/IL-SBA-15 catalysts, Au/APS-SBA-15 was the smallest in Au particle size. The size distribution and mean size of Au particles, however, were not specified therein. The Au $4f_{5/2}$ (87.9 eV) and Au $4f_{7/2}$

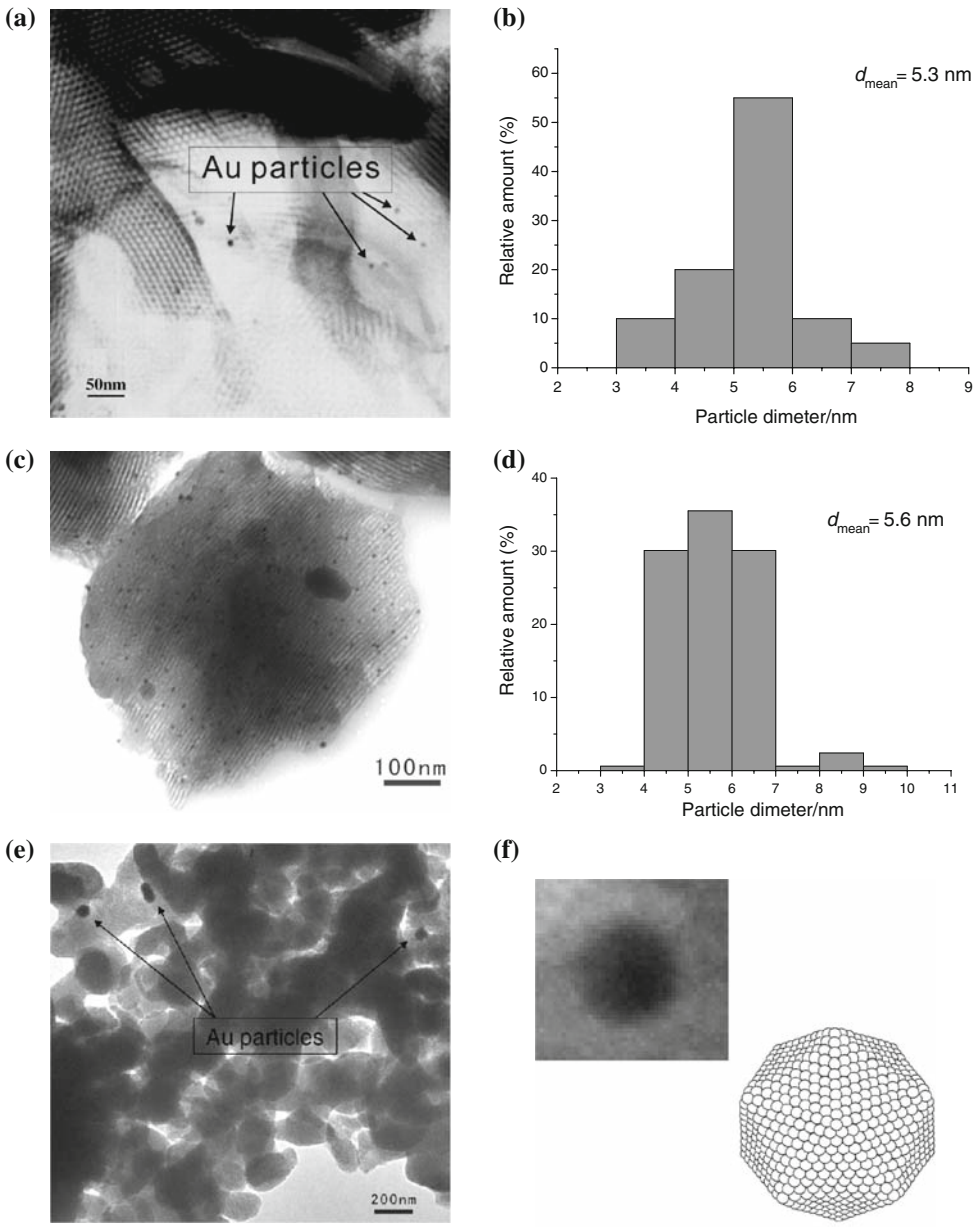

Fig. 6 TEM images as well as particle size distributions of **a**, **b** 1%Au/SBA-15, **c**, **d** 1%Au/APTS-SBA-15; **e** TEM image of 1%Au/MCM-41, and **f** icosahedral morphology of Au NPs

(84.2 eV) signals detected in XPS measurements over 1%Au/APTS-SBA-15 and 1%Au/SBA-15 (not shown) were very weak, suggesting that the Au species were mainly settled on the internal surface of SBA-15. It is believed that the walls of mesopores restrain the growth of Au particles inside the channels. From Table 1, one can see that Au NPs in the size range of 3–8 nm show nearly identical product distribution. Compared to 1%Au/SBA-15 and 1%Au/APTS-SBA-15, 1%Au/MCM-41 shows poorer dispersion of Au particles. The Au particle size of the present Au/MCM-41 catalyst is rather big (>60 nm) and located on the external surface of the support. Due to low Au loading and large Au particle size, the observed Au particles are quite limited (Fig. 6e). Therefore, the diagram of the Au particle size distribution for Au/MCM-41 is difficult to present. However, it is revealed from the TEM observation that the Au particle size of Au/MCM-41 is approximately in the range of 60–100 nm (Fig. 6e). The bulky Au particles are non-selective to the generation of CHOL and CHHP (Table 1). Lü et al. [23] reported the CHX oxidation over Au nanoparticles in mesoporous materials, mainly MCM-41. It was found that Au/MCM-41 as well as Au/SBA-15 was active for the reaction, and the former showed better performance than the latter [23]. In the present study, a CSTR of large capacity was adopted for the first time to investigate the CHX oxidation over Au-based catalysts using air-like oxidant (a mixture of 20% O_2–80% N_2). Note that different approaches have been applied for catalyst preparation in the two studies, therefore, the catalyst nature, especially the Au particle size distribution in Au/MCM-41, is largely different. The Au particle size of the Au/MCM-41 catalyst [23] was found to be considerably smaller than that of Au/MCM-41 in the present study. Nevertheless, the reaction data of both studies suggested that good catalytic performance is closely related to the presence of small-sized Au nanoparticles; and this study further indicates a clear relationship between the particle size distribution and the reaction performance. As revealed in Fig. 6a,c, the Au NPs of 1%Au/SBA-15 and 1%Au/APTS-SBA-15 are essentially spherical in shape. It is proposed that the NPs can be of icosahedral morphology (Fig. 6f) with hexagonally close-packed surface [30]. Based on such an understanding, we estimated the concentration of surface Au atoms by adopting the measured mean particle sizes [21] (an average Au particle size of 70 nm was taken for 1%Au/MCM-41) for the determination of TOFs of products.

3.2.3 XRD

Figure 7 illustrates the small-angle XRD pattern of 1%Au/SBA-15 and wide-angle XRD patterns of 1%Au/APTS-SBA-15 and 1%Au/MCM-41. The small-angle pattern shows the (110) and (200) diffraction peaks of SBA-15

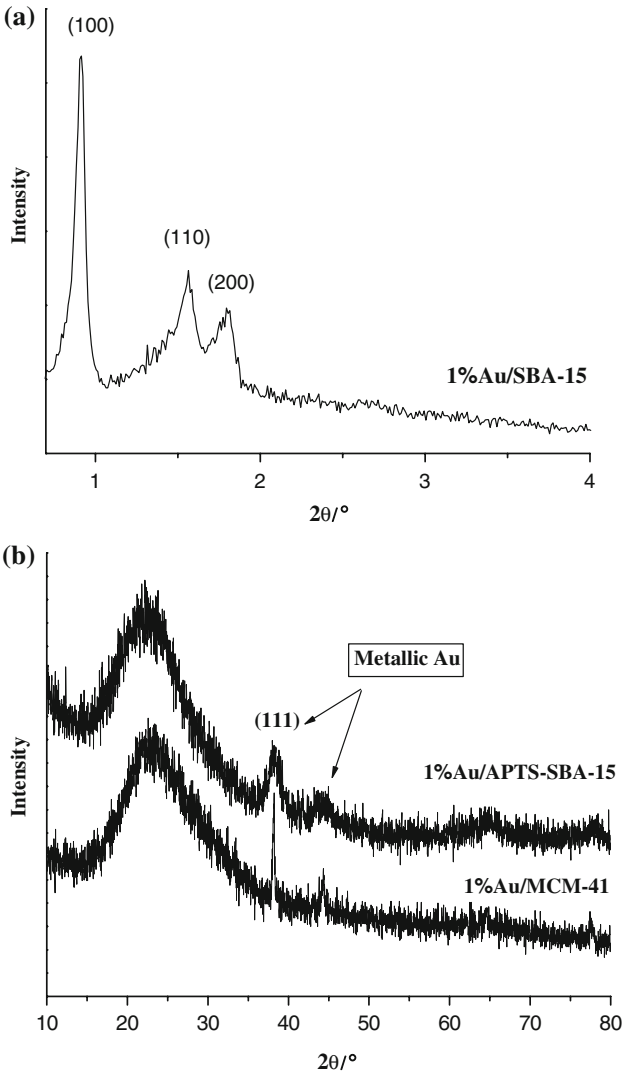

Fig. 7 **a** Small-angle XRD pattern of 1%Au/SBA-15, **b** wide-angle XRD patterns of 1%Au/APTS-SBA-15 and 1%Au/MCM-41

(Fig. 7a), indicating the retention of well-ordered hexagonal mesopore structure. The wide-angle patterns reveal the presence of metallic Au species (Fig. 7b). The crystallinity of the MCM-41 is good in view of the small angle XRD pattern of MCM-41 (not shown). One can see that the Au^0 peaks of 1%Au/MCM-41 are sharper and more intense than those of 1%Au/APTS-SBA-15, indicating that the size of Au particles of the former is bigger than that of the latter. By using the Scherrer equation, we estimated a particle size of 6.0 nm [based on the (111) peak] of Au NPs on 1%Au/APTS-SBA-15, in good agreement with the mean particle size (5.6 nm) of Au NPs derived from the TEM result.

3.2.4 Intrinsic Activity

The calculated TOFs of (CHONE + CHOL + CHHP) production over 1%Au/SBA-15, 1%Au/APTS-SBA-15,

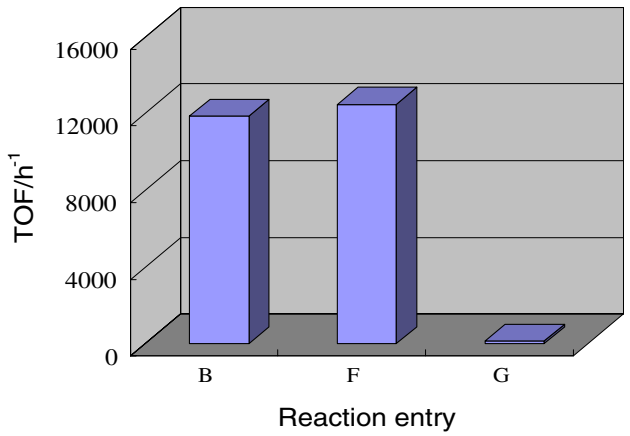

Fig. 8 Turnover frequencies (*TOFs*) of (CHONE + CHOL + CHHP) over 1%Au/SBA-15 (*Entry B*), 1%Au/APTS-SBA-15 (*Entry F*), and 1%Au/MCM-41 (*Entry G*)

and 1%Au/MCM-41 are depicted in Fig. 8. One can see that much higher TOFs are obtained over 1%Au/SBA-15 and 1%Au/APTS-SBA-15 in which Au NPs of 3–8 nm size are well dispersed on the internal surface of SBA-15. Note that TOFs of 11,000–12,000 h^{-1} are accomplished under mild reaction conditions viz. in an O_2/N_2 atmosphere similar to air (rather than pure O_2) and at system pressures of 0.6–1.0 MPa, and such a performance has not been achieved before. On the other hand, remarkably low TOF was detected over 1%Au/MCM-41 in which there was bulky Au particles on the external surface of MCM-41. In view of the significant difference in intrinsic activities, one can deduce that the CHX oxidation catalyzed by Au particles is rather size-sensitive as depicted in Scheme 1. It is thought that there are surface Au assemblies active and selective for the target reaction. The density of the assemblies, however, is particle-size dependent. The Au particles in the range of 3–8 nm are fit for generating the active assemblies, accounting for the higher activities of 1%Au/SBA-15 and 1%Au/APTS-SBA-15 in comparison to that of 1%Au/MCM-41.

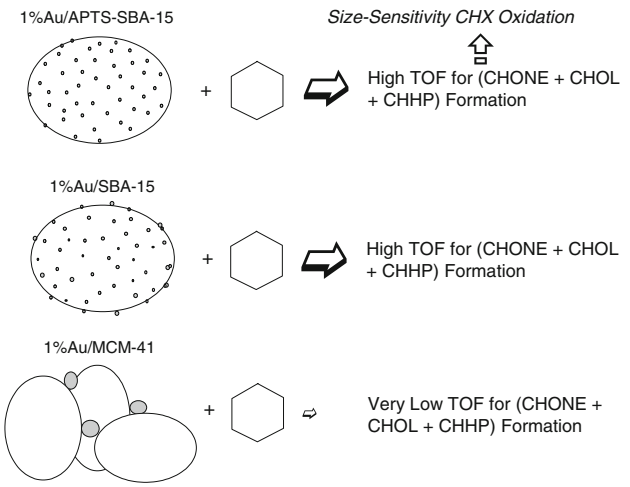

Scheme 1 Size-sensitivity of CHX oxidation over supported Au particles

4 Concluding Remarks

In the present study, we have demonstrated that the oxidation of cyclohexane can be efficiently catalyzed under mild conditions by the Au NPs (size: 3–8 nm) located uniformly on the internal walls of SBA-15. Remarkably high TOFs were achieved over 1%Au/SBA-15 and 1%Au/APTS-SBA-15 when the reaction was conducted in a continuously stirred tank reactor in an air-like atmosphere at system pressures of 0.6–1.0 MPa. Based on the results of TOFs, a size-sensitivity feature is suggested for CHX oxidation. From the engineering point of view, the use of the continuously stirred tank reactor results in accurate maintenance of system pressure as well as improvement in mixing issue, leading to quick diffusion of reactant and efficient contact of reactant, oxidant, and catalyst. Due to the possible confinement of CHX and position of Au NPs inside the SBA-15 channels, there is enhanced reaction of CHX oxidation.

Acknowledgments This work was supported by DSM Fibre Intermediates. LL would like to thank CTA for helpful guidance during her stay at HKBU.

References

1. Musser MT (1987) In: Gerhartz W (ed) Encyclopedia of Industrial Chemistry. Wiley-VCH, Weinheim, pp 217–220
2. Schuchardt U, Cardoso D, Sercheli R, Pereira R, Da Cruz RS, Guerreiro MC, Mandelli D, Spinacé EV, Pires EL (2001) Da Cruz. Appl Catal A 211:1
3. Pillai UR, Sahle-Demessie E (2002) Chem Commun 20:2142
4. Arends IWCE, Sheldon RA, Wallau M, Schuchardt U (1997) Angew Chem Int Ed Engl 36:1144
5. Spinacé EV, Pastore HO, Schuchardt U (1995) J Catal 157:631
6. Zahedi-Niaki MH, Kapoor MP, Kaliaguine S (1998) J Catal 177:231
7. Carvalho WA, Varaldo PB, Wallau M, Schuchardt U (1997) Zeolites 18:408
8. Perkas N, Wang YQ, Koltypin Y, Gedanken A, Chandrasekaran S (2001) Chem Commun 11:988
9. Raja R, Sankar G, Homas JM (1999) J Am Chem Soc 121:11926
10. Sakthivel A, Selvam P (2002) J Catal 211:134
11. Guo CC, Song JX, Chen XB, Jiang GF (2000) J Mol Catal A Chem 157:31
12. Guo CC, Liu XQ, Liu Y, Chu MF, Zhang XB (2003) J Mol Catal A Chem 192:289
13. Guo CC, Chu MF, Liu Q, Liu Y, Guo DC, Liu XQ (2003) Appl Catal A 246:303
14. Haruta M (1997) Catal Surv Jpn 1:61
15. Haruta M (1997) Catal Today 36:115
16. Akolekar DB, Bhargava SK (2005) J Mole Catal A Chem 236:77

17. Falsig H, Hovlbaek B, Kristensen IS, Jiang T, Bligaard T, Christensen CH, Nørskov IK (2008) Angew Chem Int Ed 47:4835
18. Zhang X, Corma A (2008) Angew Chem Int Ed 47:4358
19. Corma A, González-Arellano C, Lglesias M, Sánchez F (2007) Angew Chem Int Ed 46:7820
20. Ishida T, Haruta M (2007) Angew Chem Int Ed 46:7154
21. Abad A, Corma A, García H (2008) Chem Eur J 14:212
22. Zhao R, Ji D, Lu GM, Qian G, Yan L, Wang XL, Suo JS (2004) Chem Commun 7:904
23. Lu GM, Ji D, Qian G, Qi YX, Wang XL, Suo JS (2005) Appl Catal A 280:175
24. Lu GM, Zhao R, Qian G, Qi YX, Wang XL, Suo JS (2004) Catal Lett 97:115
25. Zhu KK, Hu JC, Richards R (2005) Catal Lett 100:195
26. Xu LX, He CH, Zhu MQ, Fang S (2007) Catal Lett 114:202
27. Zhao D, Feng J, Huo Q, Melosh N, Fredrickson GH, Chmelka BF, Stucky GD (1998) Science 279:548
28. Kresge CT, Leonowicz ME, Roth WJ, Vartuli JC, Beck JS (1992) Nature 359:710
29. Beck JS, Vartuli LC, Roth WJ, Leonowicz ME, Kresge CT, Schmitt KD, Chu CTW, Olson DH, Sheppard EW, McMullen SB, Higgings JB, Schlenker JC (1992) J Am Chem Soc 114:10834
30. Wang ZL (2000) In: Wang ZL (ed) Characterization of nanophase materials. Wiley-VCH, Weinheim, pp 37–80